ACS NANO

www.acsnano.org

ARTICLE

Hybrid Nanoparticle Engineered with Transforming Growth Factor -β1-Overexpressed Extracellular Vesicle and Cartilage-Targeted Anti-Inflammatory Liposome for Osteoarthritis

Jun Yong Kim,[†] Won-Kyu Rhim,[†] Seung Yeon Lee,[†] Jung Min Park, Duck Hyun Song, Seung-Gyu Cha, Sang-Hyuk Lee, Dong-Youn Hwang, Byoung Ju Kim, Seungsoo Rho, Tae-Keun Ahn, Chun Gwon Park, and Dong Keun Han*

Cite This: *ACS Nano* 2024, 18, 33937−33952

Read Online

ACCESS | Metrics & More | Article Recommendations | Supporting Information

ABSTRACT: Extracellular vesicles (EVs) possess the characteristics of their parent cells, based on which various studies have actively investigated treatments for diseases using mesenchymal stem cell-derived EVs due to their regenerative activity. Furthermore, in recent years, there have been significant efforts to engineer EVs to improve their native activities and integrate additional functions. Although both endogenous and exogenous methods are used for engineering EVs, endogenous methods may pose the problem of administering substances to cells undergoing metabolic changes, which can cause potential side effects. In addition, exogenous methods may have the limitation of losing beneficial factors inside EVs due to membrane disruption during engineering processes. Surface modification of EVs may also impair efficiency due to the presence of proteins on the EV surface. Therefore, in this study, a stable and efficient engineering method was achieved through the ethanol-mediated hybridization of EVs and functionalized lipid nanoparticles (LNPs) with a fusogenic lipid component. During hybridization, the internal bioactive factors and targeting moiety were maintained to possess the characteristics of both LNPs and EVs. The Ab-Hybrid, which was successfully synthesized through hybridization with nicotinamide-encapsulated and Col2A1 antibody-modified liposome and Transforming growth factor-β1 (TGF-β1)-overexpressed EVs, was administered to osteoarthritis (OA)-induced rats undergoing the destabilization of the medial meniscus surgery. Ultimately, the Ab-Hybrid demonstrated excellent chondroprotective and anti-inflammatory effects with targeting and long-lasting properties in OA lesions. We anticipate that this approach for manufacturing hybrid particles will serve as a valuable EV engineering method and a versatile platform technology applicable to various diseases.

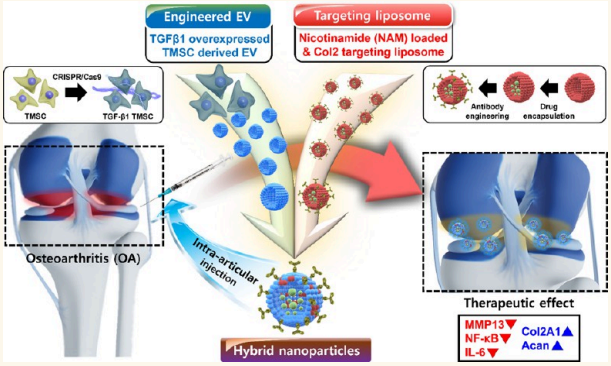

KEYWORDS: *osteoarthritis, hybrid nanoparticle, extracellular vesicles, liposome, mesenchymal stem cell*

INTRODUCTION

Osteoarthritis (OA) is a degenerative joint disease that affects numerous individuals worldwide, causing reduced quality of life due to symptoms such as pain, restricted movement, and joint deformities.[1] It is a multifaceted chronic condition that affects the entire joint, marked by inflammation, subchondral bone sclerosis, and cartilage degradation.[2] Treatments for OA have focused on pain relief rather than complete recovery of the lesion.[3] Various nonpharmacological treatments, such as

Received: June 15, 2024
Revised: November 19, 2024
Accepted: November 26, 2024
Published: December 9, 2024

https://doi.org/10.1021/acsnano.4c07992
ACS Nano 2024, 18, 33937−33952

Scheme 1. Schematic Diagram[a]

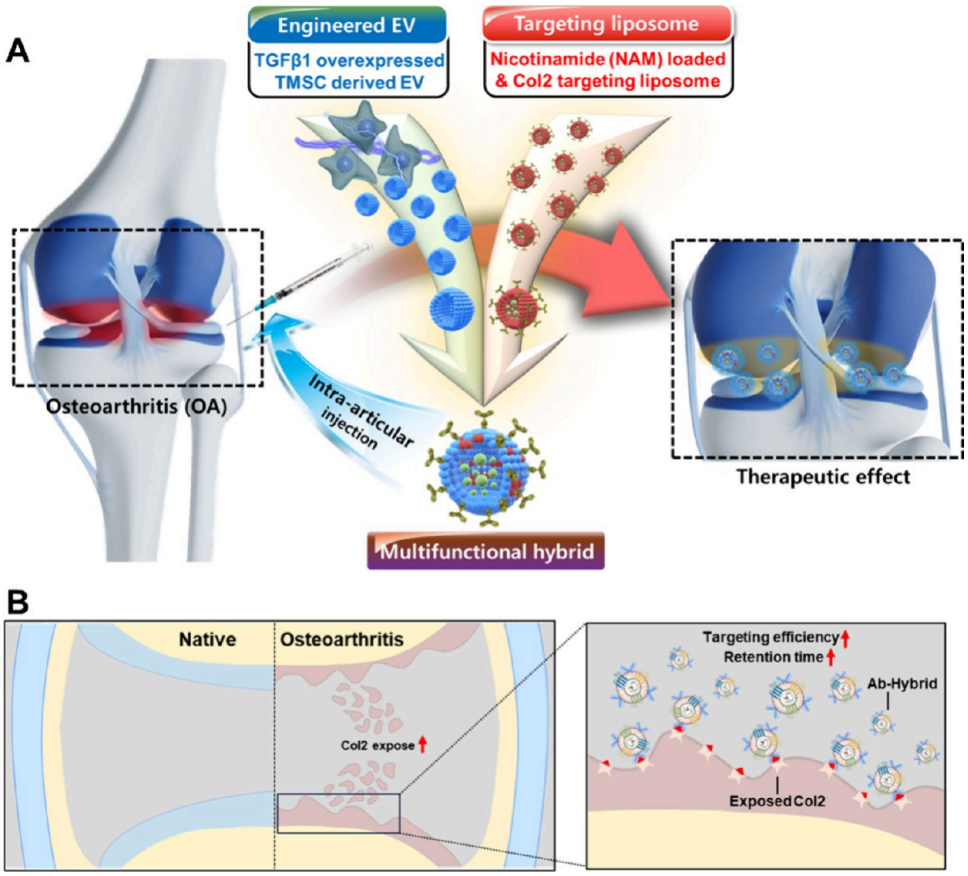

[a](A) Fabrication of hybrid nanoparticles and their application in osteoarthritis therapy. (B) Increased exposure of Col2 during the progression of osteoarthritis, along with the enhanced targeting efficiency and retention time of hybrid nanoparticles.

patient education, assistive technologies, splints, therapeutic exercises, and physical therapy, are also used to alleviate pain and improve the functional capacity of patients with OA.[4] The nonsurgical method that is frequently used in patients with OA to relieve pain is the direct injection of corticosteroids at the site of the lesion.[5,6] Steroids are not effective in treating the fundamental causes of the disease and are unsuitable for long-term treatment.[7] Moreover, steroids can reduce cartilage volume and exhibit toxicity to chondrocytes.[8,9] Hence, cell-based therapies with the implantation of stem cells or autologous chondrocytes have been proposed to overcome these issues with corticosteroids.[10,11] Although these cell-based therapies have been successful in a few cases, they require the transplantation of a large number of cells, necessitating long periods of cell culture time. Additionally, for autologous chondrocytes, significant discomforts are involved during the cell acquisition process from the patient.

Extracellular vesicles (EVs) are nanosized particles secreted by cells with various factors from cells and reflect the characteristics of their parent cells.[12,13] In particular, EVs secreted by mesenchymal stem cells (MSCs) possess regenerative capabilities, making them effective against various degeneration-related diseases.[14−17] Despite the obvious properties of EVs isolated directly from MSCs, there are limitations to their successful clinical applications.[18] Numerous engineering methods have been proposed based on endogenous and exogenous approaches to improve the original regenerative properties of EVs and provide additional functions. Endogenous engineering involves treating cells intended to produce EVs with specific substances to obtain EVs with altered characteristics by controlling preconditioning and the properties of cells.[19,20] Nevertheless, even if one aims to maintain the characteristics of the substances treated in this method, the metabolic processes of the cells can alter these characteristics, potentially compromising their efficacy and exerting adverse effects. With attempts to utilize the original bioactive substances of EVs derived from various cells, there is a growing field of research exploring the use of EVs as carriers for drug delivery systems.[21] These attempts are primarily conducted through exogenous engineering methods, which include techniques such as extrusion, sonication, electroporation, and freeze and thaw, among others.[22] However, these exogenous engineering methods result in the loss of factors contained within EVs, which makes it difficult to achieve the intact therapeutic potential of EVs. To address these challenges, a hybrid system based on the hybridization between EVs and drug-encapsulated liposomes has been proposed.[23] The core strategy of the hybrid system is to load the desired substances and modify the surface properties of the liposome, which are relatively easier to engineer than EVs, and then combine the EVs and liposomes into a single particle using various methods. Hybridization processes were initially supported by physical stimulations such as extrusion, sonication, electroporation, and freeze−thaw, but these methods did not completely overcome the limitations of exogenous engineering methods for EVs, including the loss of

https://doi.org/10.1021/acsnano.4c07992
ACS Nano 2024, 18, 33937−33952

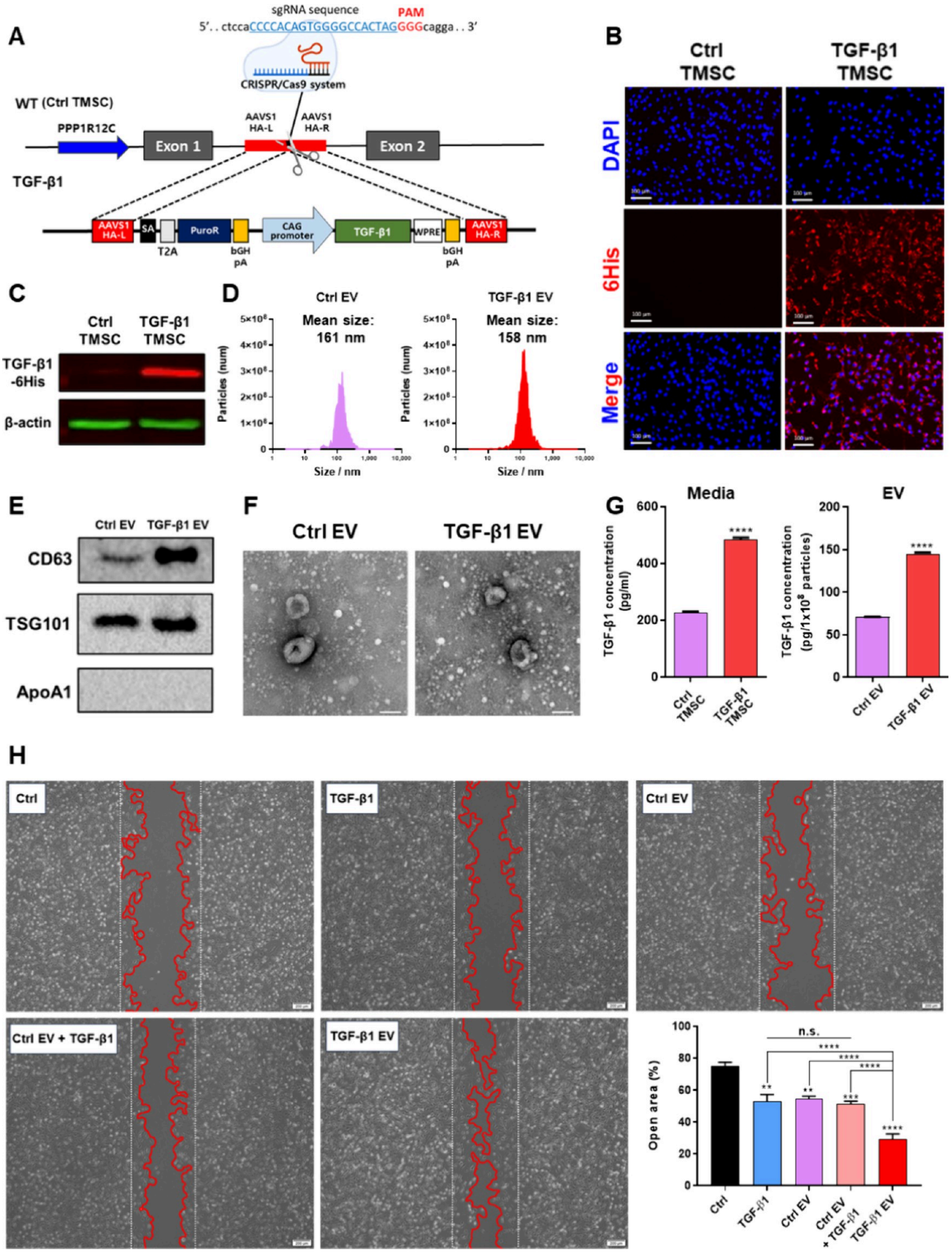

Figure 1. Confirmation of TGF-β1 overexpression in TMSC (TGF-β1 TMSC) and TGF-β1 TMSC-derived EVs. (A) Schematic representation of CRISPR/Cas9-mediated knock-in of TGF-β1 into a safe-harbor site (AAVS1) on the TMSC chromosome. Evaluation of

https://doi.org/10.1021/acsnano.4c07992
ACS Nano 2024, 18, 33937−33952

Figure 1. continued

transgenic expression of TGF-β1 with (B) immunocytochemistry and (C) Western blot analysis. (D) Size distribution of EV derived from TMSC and TGF-β1 TMSC. (E) Western blot analysis of EV derived from TMSC and TGF-β1 TMSC with EV positive markers, CD63 and TSG101, and a negative marker ApoA1. (F) Morphologies of EV imaged with TEM. Scale bars equal to 100 nm. (G) Level of TGF-β1 in cell culture media and EVs detected by ELISA. (H) Representative images of wound healing assays to evaluate wound healing effects of EVs and calculated wound healing rates of EVs (values are presented as mean ± SD (n = 3), and statistical significance was obtained with one-way analysis of ANOVA with Tukey's multiple comparison post-test (*p < 0.05; **p < 0.01; ***p < 0.001; ****p < 0.0001)).

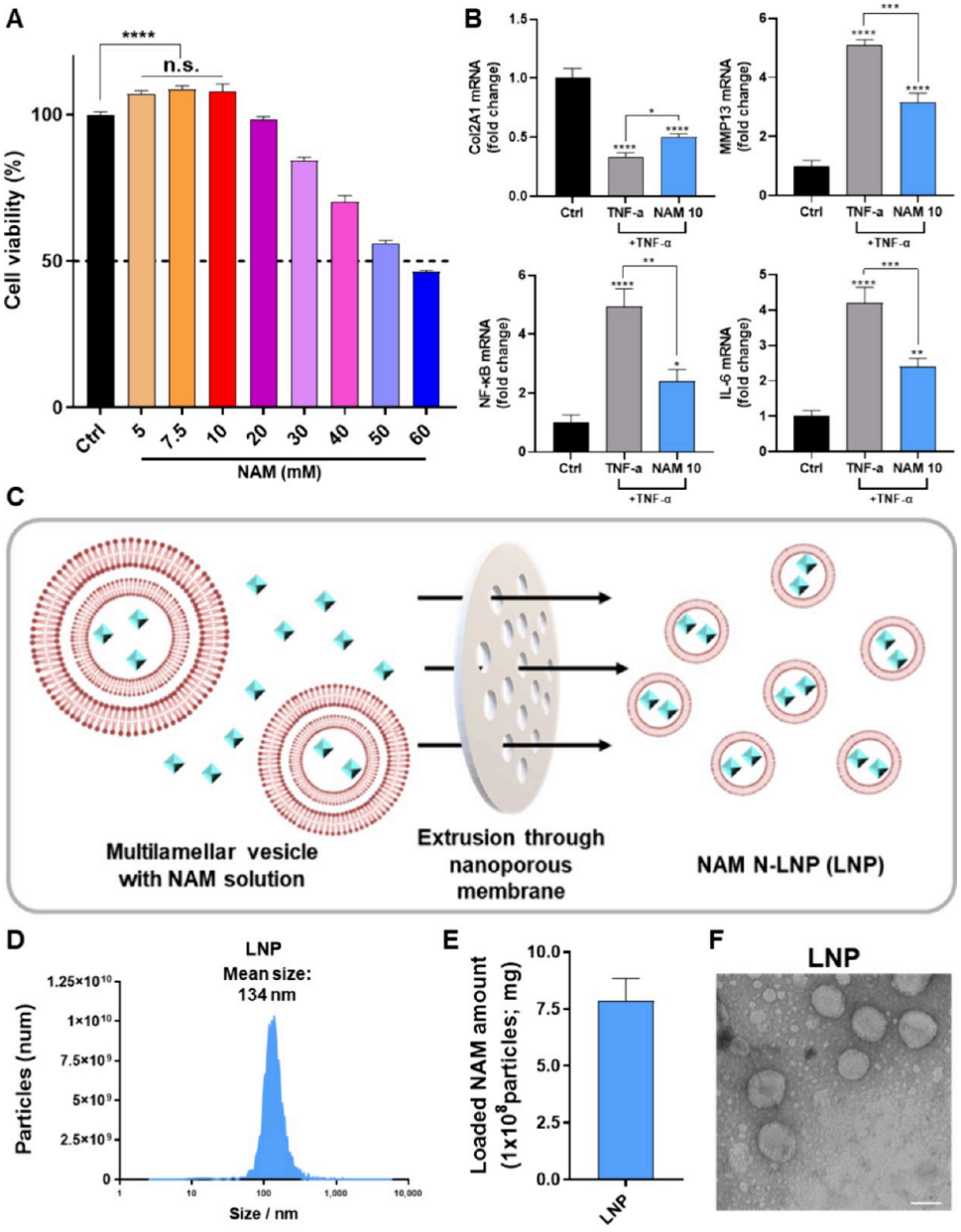

Figure 2. Nicotinamide (NAM) effect on primary rat chondrocytes. (A) Cell viability in various concentration of NAM. (B) Gene expression levels of Col2A1, MMP13, NF-kB, and IL-6. C. Illustration of the fabrication process of NAM-loaded liposome nanoparticles (N-LNP; LNP). (D) Size distribution of LNP. (E) Loaded amount of NAM in LNP quantified with HPLC. (F) Morphologies of LNP imaged with TEM. Scale bars equal to 100 nm (values are presented as mean ± SD (n = 3), and statistical significance was obtained with one-way analysis of ANOVA with Tukey's multiple comparison post-test (*p < 0.05; **p < 0.01; ***p < 0.001; ****p < 0.0001)).

internal bioactive materials. To minimize the loss of the original bioactive materials of EVs during hybridization, a strategy to control membrane fluidity with the addition of polyethylene glycol (PEG) has been introduced.[24] The PEG-mediated hybridization provided a relatively nondestructive alternative to other exogenous methods and minimized the loss of internal factors.[25] However, it was difficult to completely remove PEG, which must be resolved because of a critical problem wherein residual PEG can induce anaphylactic shock with allergic reactions.[26] Moreover, the rapid circulation of synovial fluid within the joint cavity, an environmental factor within the articular space, poses a challenge for therapeutic

https://doi.org/10.1021/acsnano.4c07992
ACS Nano 2024, 18, 33937−33952

agents to remain in the lesion site for an extended period. Therefore, biomaterial-based therapeutics have been developed to overcome the limitations of current OA treatments.[27]

In this study, we used ethanol-mediated hybridization methods to overcome these challenges and construct a multifunctional system that incorporates various bioactive factors for OA treatments.[28] Briefly, hybrid nanoparticles were fabricated by blending EVs derived from Transforming growth factor-β1 (TGF-β1)-overexpressed tonsil-derived mesenchymal stem cells (TMSCs), known for maintaining the homeostasis of cartilage tissue, and lipid nanoparticles (LNPs) encapsulating nicotinamide (NAM) and modifying collagen type II alpha 1 (Col2A1)-targeting antibody to facilitate anti-inflammatory properties and precise and long-term activities on the lesion area of OA, respectively (Scheme 1A,B). We hypothesized that the multifunctional properties of every single particle were achieved through complete hybridization between EVs and LNPs. The TGF-β1-overexpressed EVs contributed to maintaining homeostasis in the cartilage microenvironment and protecting the cartilage. Furthermore, NAM- and Col2A1 antibody-modified LNPs demonstrated anti-inflammatory effects by overcoming the rapid flow of synovial fluid on the OA lesion. Altogether, the hybrid nanoparticles proposed in this study may contribute to cartilage regeneration through the combined action of various bioactive factors.

RESULTS AND DISCUSSION

EVs Derived from TGF-β1-Overexpressed TMSCs. EVs, obtained from MSCs, have been used to promote tissue regeneration, exhibiting properties such as anti-inflammatory, antiapoptotic, and antifibrotic effects of parent cells.[29−31] To strengthen the specific function of these characteristics, TGF-β1, a key component of cartilage homeostasis, was overexpressed in TMSCs using the clustered regularly interspaced palindromic repeats/Cas9 (CRISPR/Cas9) system (Figure 1A). The CRISPR/Cas9 system is known for its high efficiency and precision,[32] and the overexpression of TGF-β1 in TMSCs was confirmed by immunocytochemistry (ICC) and Western blotting (Figure 1B,C). The TGF-β1-*His*-overexpressed TMSCs exhibited a higher amount of *His* protein expression than the negligible amount of *His* protein expression in control TMSCs. Two types of EVs, control EVs and TGF-β1 EVs, were serially isolated using the tangential flow filtration (TFF) system from control TMSCs and TGF-β1-overexpressed TMSCs, respectively. Both EVs had similar particle mean sizes and size distributions in the nanoparticle tracking analysis (NTA) (Figure 1D). The presence of the representative transmembrane protein (CD63), the intracellular protein (Tumor susceptibility gene 101; TSG101), and the major negative marker apolipoprotein A1 (Apo-A1) was evaluated by Western blotting according to the MISEV 2023 guidelines to confirm EVs (Figure 1E). EV-positive markers, namely, CD63 and TSG101, were detected, whereas the EV-negative marker Apo-A1 was not detected in both types of EV. There was also no obvious difference in their appearance, with typical cup-shaped and spherical morphologies observed in transmission electron microscope (TEM) images (Figure 1F). To confirm the amount of TGF-β1 in engineered TMSCs and their carrying capacity with EVs isolated from these cells, the expression levels of TGF-β1 in both TMSCs and EVs were evaluated by an enzyme-linked immunosorbent assay (ELISA). Results demonstrated that the amount of TGF-β1 increased by approximately two times in both TGF-β1 TMSCs and TGF-β1 EVs compared with that in native TMSCs and EVs (Figure 1G). These data indicate the successful overexpression of TGF-β1 in TMSCs through the CRISPR/Cas9 system and that the EVs reflect the characteristics of their parent cells. Based on these results, a wound healing assay was conducted to demonstrate the regenerative promoting activity of TGF-β1 using primary rat chondrocytes (PRCs) (Figure 1H). Both types of EVs (ctrl EVs and TGF-β1 EVs) were administered at the same concentration, 1×10^8 particles/mL, and the concentration of free TGF-β1 alone was matched to the amount of TGF-β1 in 1×10^8 particles/mL of TGF-β1 EVs, calculating 290 pg. For the ctrl EV + TGF-β1 group to compare the regenerative activity with separate incubation of EVs and TGF-β1, whole amounts of TGF-β1 were matched equally to 290 pg mixed with 140 pg of TGF-β1 from ctrl EVs and an additional 150 pg of free TGF-β1. The wound healing assay revealed that the TGF-β1 EV group exhibited the strongest activities, suggesting that the wound healing capacity was upregulated with MSC-derived EVs and facilitated with additional TGF-β1. The efficiency of TGF-β1 was also maximized through encapsulation in EVs by protecting TGF-β1 for an efficient intracellular delivery compared with free TGF-β1. These results are consistent with the anticipated characteristics of EVs as drug-delivery vehicles.[33] Therefore, we used TGF-β1 EVs and named them EVs in all subsequent experiments.

NAM-Encapsulated LNPs for Anti-Inflammatory Effect. NAM is a member of the vitamin B3 family and regulates inflammation in OA and other diseases.[34,35] To confirm these properties of NAM in chondrocytes, an optimum concentration of NAM in PRCs (Figure 2A). Cell viability increased up to 10 mM and decreased at >20 mM, with an LD50 between 50 and 60 mM. On the basis of these results, 10 mM NAM (NAM 10) was administered to tumor necrosis factor-α (TNF-α; 20 ng/mL)-pretreated PRCs to demonstrate the anti-inflammatory effects of NAM in an OA model mimicked *in vitro*.[36] The cartilage protection effects of NAM were analyzed by detecting the expression levels of COL2A1 for the composition of cartilage and matrix metallopeptidase 13 (MMP13) for the cartilage-degrading enzyme. Moreover, the expression levels of inflammatory factors, nuclear factor κB (NF-κB), and interleukin-6 (IL-6) were evaluated to confirm the anti-inflammatory effects of NAM (Figure 2B). The higher expression levels of COL2A1 in the NAM 10 group than those in the TNF-α-treated group indicated that NAM exerts a protective effect on cartilage. In addition, MMP13, a major factor in the vicious cycle of cartilage inflammation, was downregulated, and similarly, NF-κB and IL-6 levels were also reduced.[37] Additionally, the inhibitory effect of NAM on inflammation-induced apoptosis was confirmed through terminal deoxynucleotidyl transferase dUTP nick end labeling (TUNEL) analysis, showing a significant difference (Figure S1). Hence, these results suggest that NAM can regulate inflammation while simultaneously exerting a protective effect on the cartilage. To improve the therapeutic effects of drugs and facilitate the formation of hybrid with EVs through the fusion process, we selected fusogenic liposomes (LNPs) as a drug delivery vehicle (Figure 2C).[38−40] The LNPs were manufactured using the thin film hydration method followed by the extrusion method, and the size of the manufactured LNPs was measured using a MONO ZetaView (Figure 2D). The amount of NAM loaded into the LNPs was quantified at

https://doi.org/10.1021/acsnano.4c07992
ACS Nano 2024, 18, 33937−33952

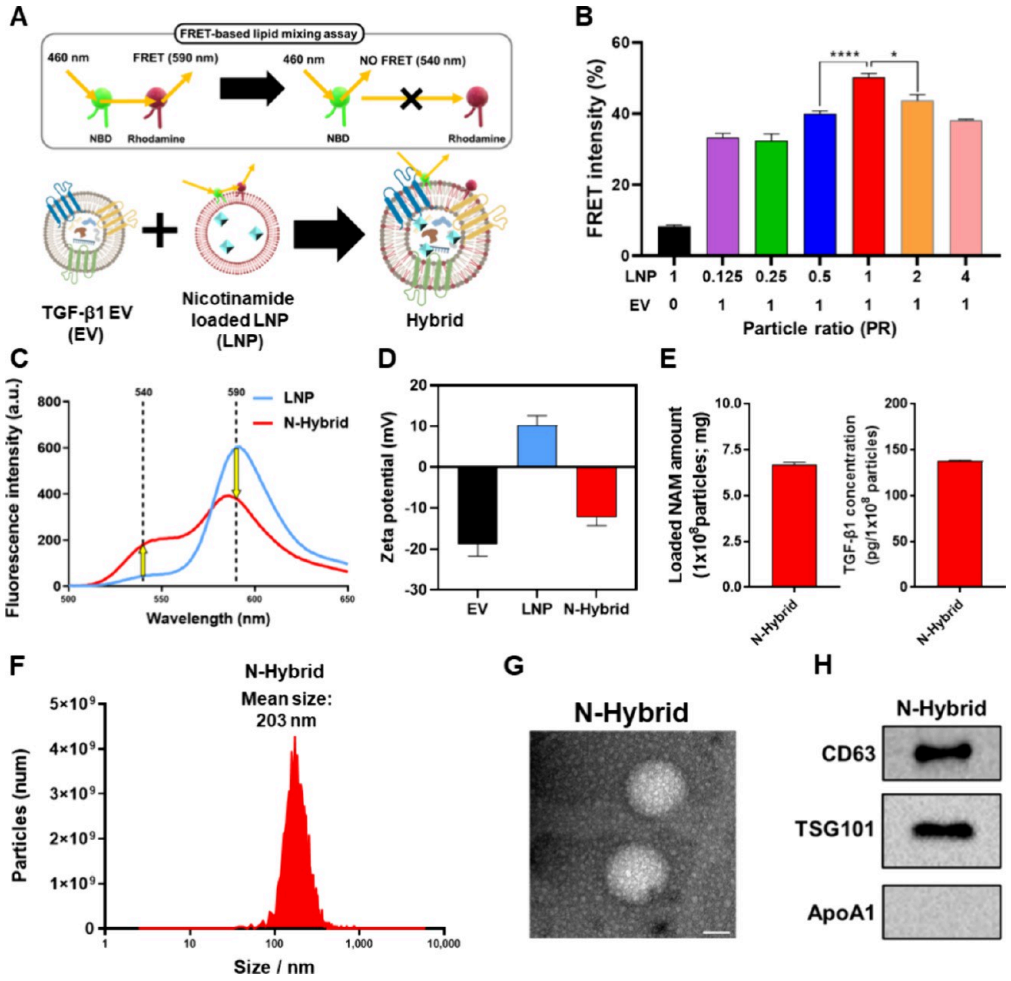

Figure 3. Ethanol-mediated hybridization between EVs and LNPs. (A) Illustration of the FRET-based lipid mixing assay. (B) FRET intensity in various EV and LNP particle ratios (PRs). (C) Changes in fluorescence intensity at each wavelength during EV-LNP hybridization. (D) Zeta potential of EV, LNP, and N-Hybrid. (E) Loaded amount of NAM and TGF-β1 in N-Hybrid quantified with HPLC and ELISA, respectively. (F) Size distribution of N-Hybrid. (G) Morphologies of N-Hybrid imaged with TEM. Scale bars equal to 100 nm. (H) Western blot analysis of N-Hybrid with EV positive markers, CD63 and TSG101, and a negative marker, ApoA1 (values are presented as mean ± SD (n = 3), and statistical significance was obtained with one-way analysis of ANOVA with Tukey's multiple comparison post-test (*p < 0.05; **p < 0.01; ***p < 0.001; ****p < 0.0001)).

7.9 mg/1 × 10^8 particles by high-performance liquid chromatography (HPLC) (Figure 2E and Figure S2). Moreover, the resulting TEM images confirmed the typical spherical morphology of the liposomes with a size of approximately 100 nm (Figure 2F). Based on these data, the successful production of NAM-encapsulated LNPs was confirmed.

Fabrication of the EV−LNP Hybrid Nanoparticle. Although various engineering approaches have been proposed in recent years to provide additional functions for EVs,[41] many of these methods involve the loss of significant internal factors within the EVs. Therefore, to minimize such loss of internal factors while achieving engineering, an engineering strategy involving the induction of hybridization between EVs and LNPs has been proposed. In particular, the strategy of inducing hybridization by controlling the fluidity of lipid membranes is attracting attention as a method that does not utilize external mechanical stimulations. Initially, PEG was used to increase the membrane fluidity and the close contact of the lipid membrane to trigger the reorganization of lipid molecules. However, removing the free PEG, which may cause allergic reactions, was challenging.[42,43] Therefore, we used the ethanol-mediated hybridization strategy to eliminate the possibility of side effects caused by additives.[44] Ethanol was used to increase the fluidity of the lipid membrane of both EVs and LNPs.[45] To confirm hybridization, a förster resonance energy transfer (FRET)-based lipid mixing assay was introduced (Figure 3A). This method depends on changes in the intensity of light with energy transfer between donor (NBD) and acceptor (rhodamine) fluorophores on the LNPs as changing the distance between these fluorophores during hybridization with EVs.[46] Based on this hybrid validation method, the FRET intensity was identified at various ratios of EVs to LNPs (Figure 3B). The FRET intensity was approximately 50% at a 1:1 ratio, exhibiting statistical significance compared to other particle ratio (PR) groups. Using these results, we optimized the ratio of LNPs to EVs to 1:1 for complete and efficient fusion between them. When we compared the light intensity of 1:1 PR and LNPs measured at 1 nm intervals across the spectra of wavelengths, we detected significant changes at 540 nm, the emission peak of NBD (donor), and at 590 nm, the emission peak of rhodamine (acceptor). Through hybridization, the altered spectral results showed increased intensity in the emission peak for NBD, 540 nm, and, conversely, decreased intensity in the emission peak for rhodamine, 590 nm, with

https://doi.org/10.1021/acsnano.4c07992
ACS Nano 2024, 18, 33937−33952

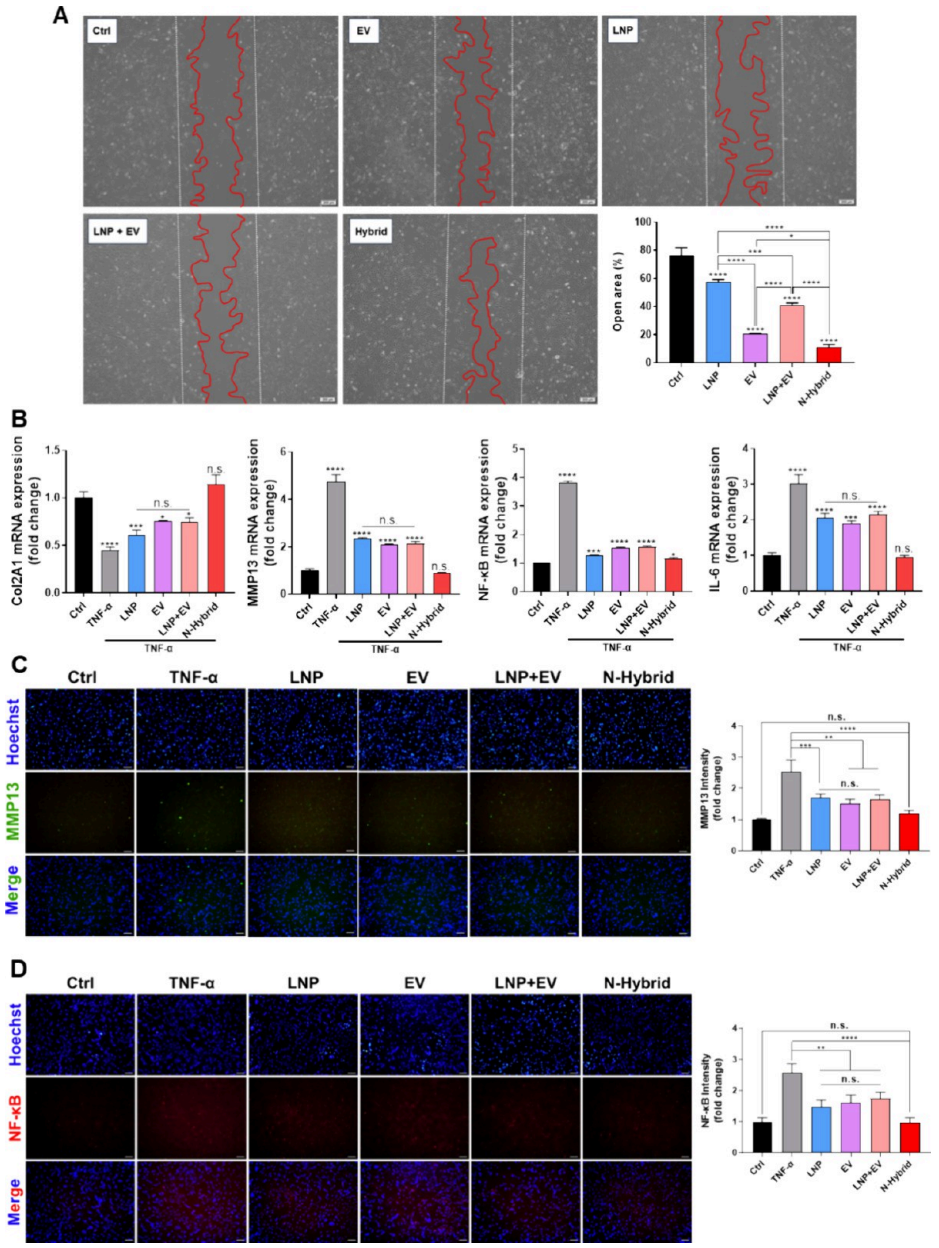

Figure 4. Functionality of hybrid nanoparticle. (A) Representative images of wound healing assays to evaluate wound healing effects of EV, LNP, and N-Hybrid, and quantification data for wound healing rates of EV, LNP, and N-Hybrid. (B) Gene expression levels of Col2A1, MMP13, NF-kB, and IL-6. (C) Fluorescence-based immunocytochemistry for MMP13 expression. (D) Fluorescence-based immunocytochemistry for NF-κB expression (values are presented as mean ± SD (n = 3), and statistical significance was obtained with one-way analysis of ANOVA with Tukey's multiple comparison post-test (*p < 0.05; **p < 0.01; ***p < 0.001; ****p < 0.0001)).

decoupling FRET (Figure 3C). Furthermore, the positively charged LNPs changed to slightly negatively charged with hybrid formation (N hybrid) using negatively charged EVs (Figure 3D). To confirm whether the internal bioactive components of EVs and LNPs remained intact after hybrid formation, we evaluated the loading amount of TGF-β1 and NAM of the hybrid by HPLC and ELISA (Figure 3E). We detected 137 pg/1 × 10^8 particles of TGF-β1 and 6.7 mg/1 × 10^8 particles of NAM in the N-Hybrid, which confirmed that the substances inside LNPs and EVs were retained with minimal loss in the N-Hybrid compared with the initial amount of TGF-β1 and NAM in EVs and LNPs as shown in Figures 1G and 2E. These findings confirmed that the ethanol-mediated fusion is an emerging strategy that minimizes the loss of the internal components of EVs and LNPs while maintaining the respective functionalities.[47] Regarding the size examined using MONO ZetaView, we observed that the average size increased to 203 nm for the N-Hybrid (Figure 3F); an increase in size indicates the indirect confirmation of fusion between the two nanovesicles. A distinct morphology different from that of both EVs and LNPs was displayed with a size of approximately 200 nm for the N-Hybrid in the TEM analysis (Figure 3G).[48] The ethanol-mediated hybridization approach regulates membrane fluidity to induce fusion between the respective vesicles. As a result, unlike conventional EV engineering methods that utilize external forces to disassemble and reassemble the membrane sequentially, which do not significantly alter particle size, ethanol-mediated

https://doi.org/10.1021/acsnano.4c07992
ACS Nano 2024, 18, 33937−33952

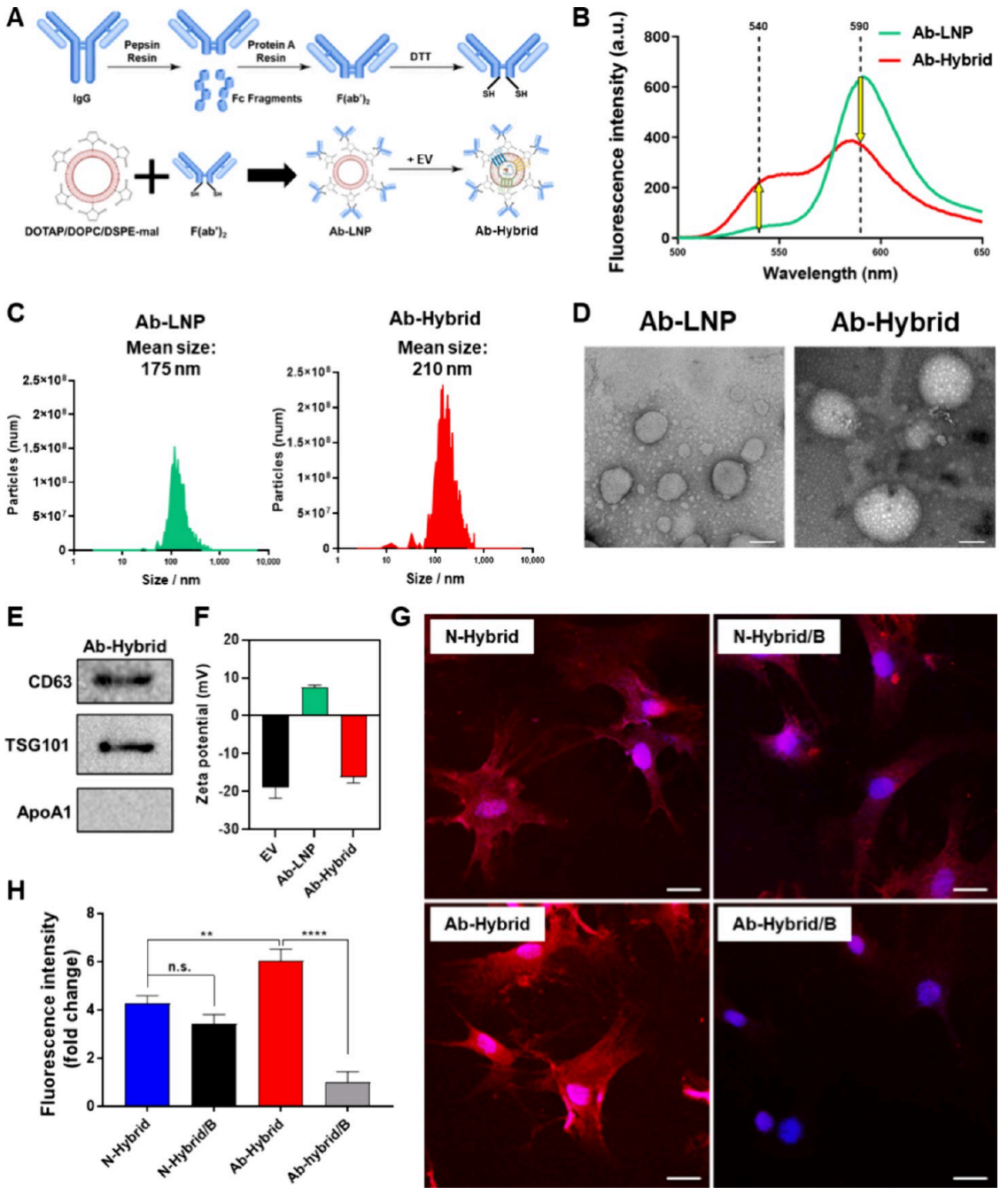

Figure 5. Antibody engineering for functionalization of hybrid. (A) Illustration of antibody engineering process and Ab-Hybrid. (B) Change in fluorescence intensity at each wavelength during hybridization of EV and Ab-LNP. (C) Size distribution of Ab-LNP and Ab-Hybrid. (D) Morphologies of Ab-LNP and Ab-Hybrid imaged with TEM. Scale bars equal to 100 nm. (E) Western blot analysis of Ab-Hybrid with EV positive markers, CD63 and TSG101, and a negative marker, ApoA1. (F) Zeta potential of EV, Ab-LNP, and Ab-Hybrid. (G) Represented images visualizing the internalization of particles at primary rat chondrocytes (PRCs). Scale bars equal to 50 μm. (H) Quantitative value of the fluorescence intensity of particles attached to the PRC (values are presented as mean ± SD (n = 3), and statistical significance was obtained with one-way analysis of ANOVA with Tukey's multiple comparison post-test (*p < 0.05; **p < 0.01; ***p < 0.001; ****p < 0.0001)).

hybridization can lead to an increase in the average size of hybrid nanoparticles as the membranes of individual vesicles fuse and become into one vesicle.[49,50] Finally, we detected the representative EV markers by Western blotting to confirm whether the characteristics of EVs were maintained even after N-hybrid formation (Figure 3H). Results revealed the expression of the positive markers of EV, CD63, and TSG101, whereas the negative marker of EV, ApoA1, was not detected. Through validation of TSG101 expression, an internal marker of EVs, we could indirectly reveal again that the internal factors of EVs are maintained through the ethanol-mediated hybridization process (Figure S4).

Functionality of the Hybrid Nanoparticle (N-Hybrid). A wound healing assay was conducted on PRCs to confirm the excellence of the N-Hybrid for regeneration. All groups were treated with the same number of total particles with LNPs,

https://doi.org/10.1021/acsnano.4c07992
ACS Nano 2024, 18, 33937−33952

EVs, a simple mix of LNPs and EVs, and N-Hybrid at a concentration of 1×10^8 particles/mL. For parallel comparisons for LNP + EV, 5×10^8 particles/mL of each particle were treated. After 24 h of particle treatment, a quantification of the open area revealed that the N-Hybrid group had the smallest open area, showing a slight difference compared with that in the EV group. These findings may be attributed to various factors inside the EVs that play a major role in wound healing and the NAM of LNPs that plays a supporting role (Figure 4A). In the PRCs pretreated with TNF-α for mimicking OA in an *in vitro* system, the expression level of Col2A1 in the N-Hybrid group was comparable to that in the ctrl group, demonstrating significant cartilage protection due to the combined action of NAM and TGF-β1 (Figure 4B). Moreover, the expression of the cartilage-degrading enzyme, MMP13, was reduced, and similar patterns of downregulation were observed for the expression of the proinflammatory markers NF-κB and IL-6. In addition to the results of gene expression, we conducted an ICC analysis of MMP13 and NF-κB levels to confirm the anti-inflammatory effects of N-Hybrid at the protein level. When the cartilage is damaged, inflammation is triggered, causing an increase in the level of MMP13 production. This results in the breakdown of cartilage collagen, which in turn exacerbates inflammation, generating a vicious cycle that is widely recognized as the progression of OA.[51] As anticipated, both MMP13 and NF-κB expressions were significantly inhibited in the groups treated with N-Hybrid nanoparticles (Figure 4C,D, respectively). The consistent results at both gene and protein levels suggest that the N-Hybrid exerted both cartilage protection and anti-inflammatory effects with superior drug delivery capabilities compared with those of EVs or LNPs alone and the simple mix of EVs and LNPs.

Surface Engineering of Hybrid Nanoparticles. In general, treatment strategies for OA involve methods for overcoming the rapid wash-out of synovial fluid within the joint cavity for prolonged residence.[52] Therefore, we aimed to modify Col2A1 antibodies on the surface of N-Hybrid particles to allow them to remain in the lesion area for a longer time (Figure 5A). Although Col2A1 is known to be expressed in various tissues, cartilage is a major tissue that contains relatively large amounts of it.[53,54] Col2A1 specifically targets collagen type II (Col2), which is exposed on the cartilage surface with the progression of OA.[55] To generate the Col2A1 antibody-functionalized hybrid (Ab-Hybrid), we used maleimide-incorporated DSPE (mal-DSPE) to create LNPs. For maximizing the targeting efficiency of the antibody, the $F(ab')_2$ fragment of Col2A1 antibody was produced using pepsin resin and thiol groups were exposed using DTT to enable conjugation with maleimide on the surface of LNPs. The $F(ab')_2$ fragment has a better targeting efficiency than intact antibodies.[56] Through this process, Col2A1 $F(ab')_2$ was synthesized to react with maleimide-incorporated LNPs, resulting in the production of antibody-decorated LNPs (Ab-LNP). Serially, the Col2A1 antibody-functionalized hybrid (Ab-Hybrid) was synthesized by ethanol-mediated hybridization as previously described, and the FRET assay revealed the successful formation of the hybrid even with the introduction of Col2A1 $F(ab')_2$ (Figure 5B). The sizes of Ab-LNP and Ab-Hybrid particles were measured using MONO ZetaView. With Col2A1 $F(ab')_2$ functionalization, the average size slightly increased in both Ab-LNP and Ab-Hybrid, but the morphologies showed no significant differences compared with those of N-LNP and N-Hybrid (Figure 5C,D). Furthermore, to confirm whether Ab-Hybrid retains the characteristics of the original EVs, we evaluated the EV markers CD63, TSG101, and ApoA1 by Western blotting. Results demonstrated that the surface functionalization of LNPs did not cause the loss of EV characteristics during hybridization with EVs, and the expression of an EV marker, TSG101, also indirectly confirmed that the internal factors of EVs were maintained during the formation of Ab-Hybrid (Figure 5E and Figure S4). The positively charged Ab-LNPs changed to negatively charged due to hybridization similar to that during N-hybrid formation (Figure 5F). The targeting property of Col2A1 $F(ab')_2$ functionalization was confirmed by the internalization of dye-labeled hybrid particles in PRCs. With Col2A1 $F(ab')_2$ modification, the hybrid particles were internalized into PRCs through Col2A1 receptors. Moreover, in cells where the Col2A1 receptors were blocked by free Col2A1, the N-Hybrid exhibited no difference in internalization efficiency compared with that in nonblocked PRCs; however, a negligible intensity was shown for Ab-Hybrid in free antibody-blocked PRCs, although intense signals were exposed in nonblocked PRCs (Figure 5G,H). These findings show that the Ab-Hybrid might target specifically the lesion site and exhibit prolonged retention at the lesion site of OA compared with the N-Hybrid.

Affinity of Hybrid Nanoparticles to OA Lesions. Based on the specificity of the Ab-Hybrid to PRCs at the cellular level, we performed *ex vivo* tests to compare the affinity of hybrid nanoparticles in actual tissues. To mimic the OA condition in an *ex vivo* model, femoral condyles isolated from 8 week old Sprague–Dawley (SD) rats were subjected to 1 h injury using 0.25% trypsin-EDTA (TE) buffer. Exposing cartilage regions to trypsin is known to mimic the pathological lesions of OA.[57] The fluorescent-labeled hybrid particles were exposed to the *ex vivo* model for 1 h and imaged using a fluorescence-labeled organism-bioimaging instrument (FOBI) (Figure 6A and Figure S5). The imaging results revealed a significant difference in intensity between the Ab-Hybrid and N-Hybrid, visible to the naked eye and clearer with rainbow intensity images. For a precise comparison of intensity, we quantified the intensity using the ImageJ program and normalized it to the size of each tissue for graphical representation (Figure 6B). Results revealed a higher fluorescence signal in the Ab-Hybrid group, similar to findings at the cellular level, indicating the prolonged retention properties of the Ab-Hybrid compared with those of the N-Hybrid at the pathological sites for improved therapeutic potentials. Based on the previous results, *in vivo* particle tracking was performed to confirm whether Ab-Hybrid shows improved targeting efficiency and retention time compared to those of N-Hybrid. After labeling particles with DiD, the labeled particles were injected into the joint cavity in the DMM model. The distribution and fluorescence intensity of the particles were observed for 30 days (Figure 6C,D). While the N-Hybrid showed fluorescence intensity outside the joint cavity, the Ab-Hybrid remained localized within the joint cavity in the initial time. This indicated an improved targeting efficiency for Ab-Hybrid compared to N-Hybrid. The fluorescence signal initially started to diminish in the joint cavity for N-Hybrid, and completely disappeared at 30 days, whereas a strong fluorescence signal was maintained for 30 days in the joint cavity for Ab-Hybrid, suggesting that N-Hybrid was cleared from the joint cavity faster than Ab-Hybrid

https://doi.org/10.1021/acsnano.4c07992
ACS Nano 2024, 18, 33937−33952

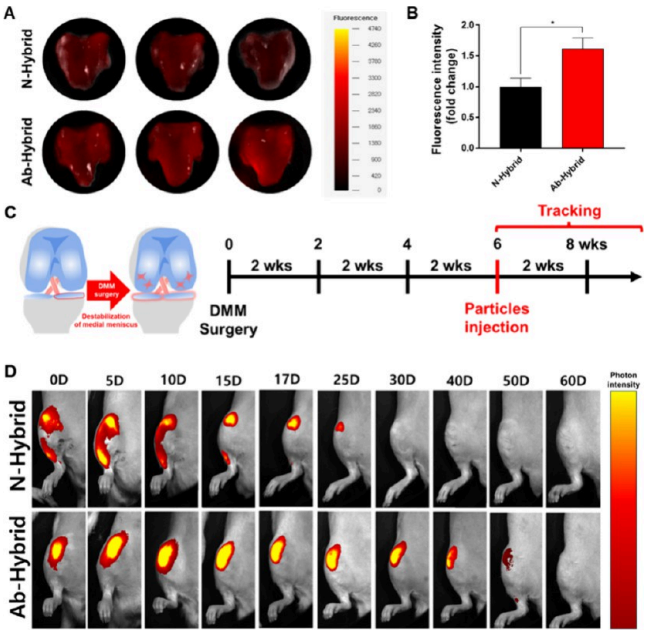

Figure 6. ***Ex vivo*** **and** ***in vivo*** **particle tracking study with N-Hybrid and Ab-Hybrid. (A) Image of particle affinity with damaged femoral condyle imaged with fluorescence-labeled organism-bioimaging instrument (FOBI). (B) Quantitative graph of fluorescence intensity. (C) Illustrated image of DMM surgery and the time schedules of** ***in vivo*** **particle tracking analysis. (D) Time-dependent knee images of rats injected with DiD-labeled N-Hybrid and Ab-Hybrid 6 weeks after DMM modeling (values are presented as mean ± SD (*n* = 3), and statistical significance was obtained with one-way analysis of ANOVA with Tukey's multiple comparison post-test (**p* < 0.05; ***p* < 0.01; ****p* < 0.001; *****p* < 0.0001)).**

despite the same amounts of particles being injected. In the Ab-Hybrid group, the fluorescence signal completely disappeared at 60 days after injection. These proved the specific targeting activity and long retention time of Ab-Hybrid to offer enhanced therapeutic efficacy compared to N-Hybrid.

In vivo therapeutic effects of Ab-Hybrid nanoparticles on the DMM-induced OA rat model. To confirm the therapeutic effects of the hybrid nanoparticles in an animal model with cartilage damage, we induced the surgical destabilization of the medial meniscus (DMM) in 8-week-old SD rats. The animal model was created with minimal incision according to a well-established protocol (Figure S6).[58] At every 2 weeks after the DMM surgery, the two types of hybrid nanoparticles, N-Hybrid and Ab-Hybrid, were administered through intra-articular (IA) injection, and the animal models were sacrificed at 8 weeks after surgery (Figure 7A). During the 8 weeks of DMM surgery and hybrid nanoparticle treatments, there were no significant weight changes among the groups (Figure S7A,B). The legs of euthanized SD rats, including the regions of the DMM surgery and particle injection, were harvested and embedded in paraffin followed by sectioning at a thickness of 10 μm. The sectioned samples were serially stained with hematoxylin and eosin (H&E) and Safranin O-fast green (S/O) for histological evaluation. Histological analysis with H&E staining revealed a relatively thicker cartilage and a larger number of chondrocytes in the groups treated with N-Hybrid and Ab-Hybrid than in the DMM group.[59] Moreover, the S/O staining revealed the presence of red-stained cartilage areas in all groups except in the DMM group. In detail, the red-stained area that reflects the proteoglycan content of cartilage was visualized in both N-Hybrid and Ab-Hybrid groups, although a less intense signal was observed compared with that in the ctrl group.[60] Based on this finding, it can be concluded that the N-Hybrid and Ab-Hybrid treatments exerted a relative cartilage-protective effect compared to the DMM surgery (Figure 7B). Moreover, the normal arrangement of cartilage can be characterized by layers stained with red and green by S/O staining.[61] Unlike that in the Ab-Hybrid group, the N-Hybrid group demonstrated a mixed pattern with a disrupted layer, indicating a disruption or alteration of the normal cartilage structure.[62] In contrast, the Ab-Hybrid group maintained a distinct layered structure in S/O staining, implying relatively normal and healthy tissues. These histological findings indicate that the intensity of S/O staining appeared similar between the N- and Ab-Hybrid groups. However, in terms of the Osteoarthritis Research Society International (OARSI) score based on the pattern of layers, which indicates the structural state of the cartilage, the Ab-Hybrid group showed a lower score than the N-Hybrid group (Figure 7C).[63] Therefore, Ab-Hybrid exerted relatively superior cartilage protection and regeneration effects than N-Hybrid.

In Vivo **Gene and Protein Expression for Ab-Hybrid Nanoparticles in the DMM-Induced OA Rat Model.** We examined the expression of cartilage-regeneration-related factors at the gene level (Figure 7D). The expression of Col2A1, a major component of cartilage, can be used as an indicator of cartilage damage,[64] increasing significantly in the DMM model treated with Ab-Hybrid. In contrast, treatment with the Ab hybrid exerted relatively high inhibitory effects on the expression of MMP13, NF-κB, and IL-6. The large difference in gene expression levels between the N-Hybrid and Ab-Hybrid groups is due to the specificity of the Col2A1 antibody to the lesion site and the ability to withstand the rapid wash-out of synovial fluid in the joint cavity. Due to similar reasons, the Ab-Hybrid exerted relatively high inhibitory effects on the expression of MMP13, NF-κB, and IL-6. Based on these gene-level results, we conducted confirmatory assessments at the protein level for Col2A1 and MMP13, a major component in cartilage and a major contributor to cartilage degradation and OA induction, respectively (Figure 7E).[65] For the parallel comparison, we normalized the expression levels of both factors using the expression of β-actin as a house keeping gene (Figure 7F). Results demonstrated that the intensity of Col2A1 was upregulated in the N-Hybrid group and maximized in the Ab-Hybrid group. Conversely, the MMP13 expression was reduced in the N-Hybrid group and minimized in the Ab-Hybrid group, suggesting relatively superior cartilage protection, regeneration, and anti-inflammatory effects of Ab-Hybrid than those of N-Hybrid. Therefore, we believe that Ab-Hybrid can be used as a promising therapeutic agent for OA, exhibiting significant efficacy.

CONCLUSIONS

This study describes a fabrication technology for hybrid nanoparticles that possess the characteristics of both EVs and LNPs simultaneously, providing an excellent therapeutic property for OA. The hybrid approach was effective in overcoming the limitations of both endogenous and exogenous methods for engineering EVs, and the difficulties in surface engineering caused by the presence of proteins on the EV

https://doi.org/10.1021/acsnano.4c07992
ACS Nano 2024, 18, 33937−33952

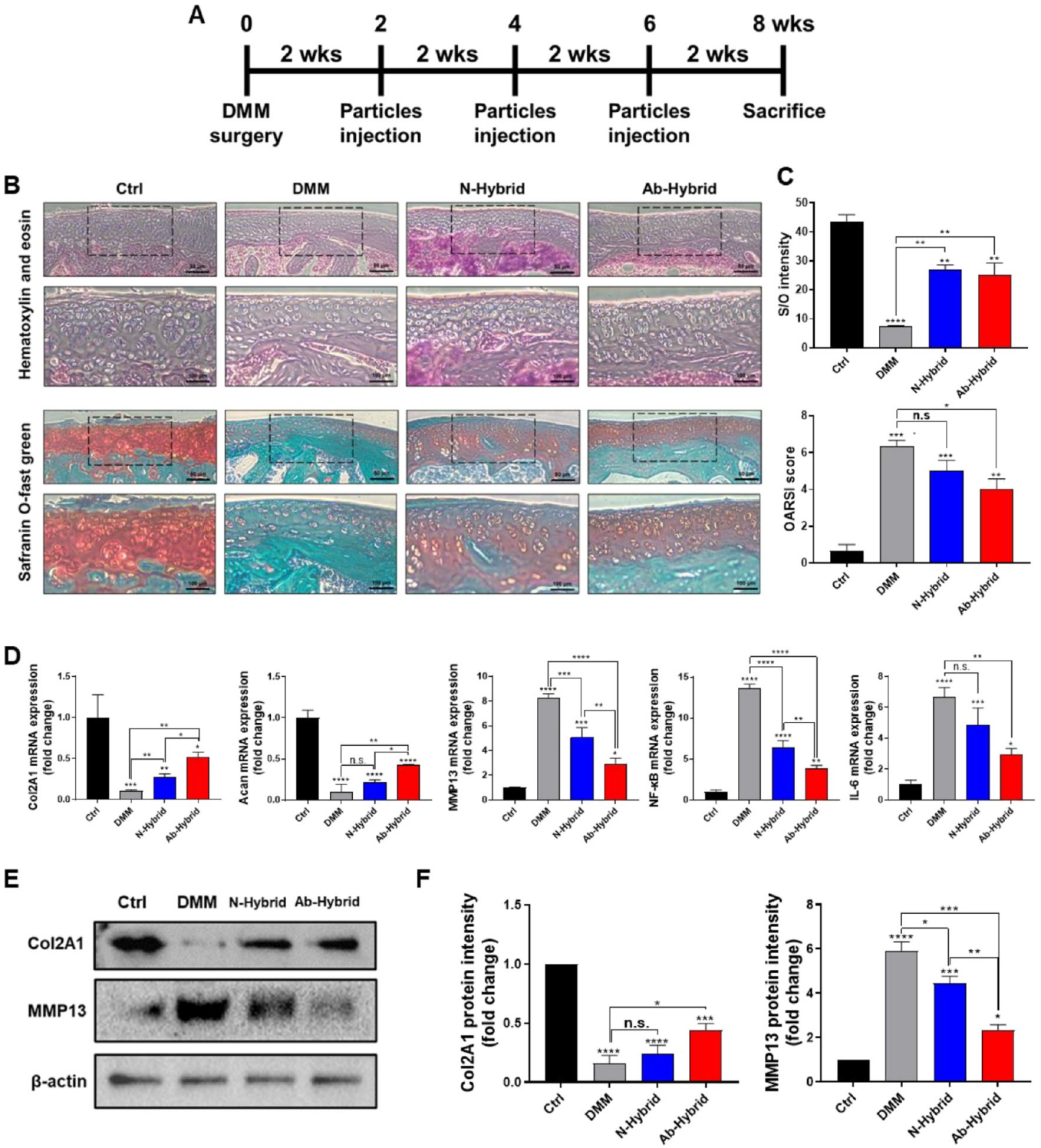

Figure 7. Histological image and gene/protein expression levels of the in vivo analysis. (A) Time schedules of *in vivo* analysis. (B) Representative images of the hematoxylin and eosin (H&E) and safranin O-fast green (S/O) staining of the samples collected at 8 weeks of postsurgery. (C) Quantitative graph of S/O staining intensity and OARSI score based with histological image. (D) Gene expression levels of the *in vivo* samples of 8 weeks postsurgery. (E) Western blot analysis for the *in vivo* samples 8 weeks after surgery. (F) Quantitative intensity graph of the Col2A1 and MMP13 normalized with β-actin intensity (values are presented as mean ± SD (n = 3), and statistical significance was obtained with one-way analysis of ANOVA with Tukey's multiple comparison post-test (*p < 0.05; **p < 0.01; ***p < 0.001; ****p < 0.0001)).

surface were resolved. The disadvantages of mechanical stimulation and PEG-mediated hybridization, viz., the loss of internal factors and severe allergic reactions due to PEG, could be overcome through ethanol-mediated hybridization using the fusogenic lipid component.

The hybrid nanoparticles in this study, Ab-Hybrid, exerted an inhibitory effect on the expression of MMP13, a key inducer

https://doi.org/10.1021/acsnano.4c07992
ACS Nano 2024, 18, 33937−33952

of OA, resulting in the downregulation of inflammatory mediators such as NF-κB and IL-6. Moreover, the combinatory effects of NAM and TGF-β1 encapsulated in the hybrid nanoparticles upregulated the expression of Col2A1, providing evidence of chondroprotective effects. The inhibitory effect of these hybrid nanoparticles on OA was demonstrated not only in *in vitro* but also in *in vivo* rat models induced with OA through DMM surgery. Furthermore, the highly specific Col2A1 antibody-functionalized Ab-Hybrid overcame rapid synovial fluid turnover in the joint cavity and exhibited superior therapeutic efficacy than the N-Hybrid. These results suggest that the ethanol-mediated fabrication technology for manufacturing hybrid nanoparticles can be used as a versatile platform technology for EV engineering and applied to diverse diseases.

MATERIALS AND METHODS

Cell Culture. Human tonsil-derived mesenchymal stem cells (TMSCs) and TGF-β1 overexpressed human tonsil-derived mesenchymal stem cells (TGF-β1 TMSCs) were presented from the Dong-Youn Hwang's Laboratory in CHA University and cultured using CellCor CD MSC media (CDM; Xcell Therapeutics, Seoul, Korea) with 1% antibiotic-antimycotic solution. All types of MSCs were seeded 5×10^5 cells/plate on a 150 pi plate. The primary rat chondrocyte (PRC; presented by Dr. Byoung Ju Kim) were cultured using DMEM-F12 (Gibco, MD, USA) media with 1% antibiotic-antimycotic solution and 10% fetal bovine serum (FBS). All types of cells were incubated at 37 °C in a humidified environment with 5% CO_2.

Cell Viability Test. Cell viability was assessed using a cell counting kit-8 (CCK-8; Dojindo, Kumamoto, Japan). The CCK-8 assay was performed according to the manufacturer's guidelines to evaluate relative cell viability. Absorbance was measured at 450 nm by using a microplate reader (Molecular Devices, CA, USA).

Isolation of Extracellular Vesicles (EVs). Conditioned media were collected every 24 h for a total duration of 120 h to isolate the EVs. To remove nonexosomal large particles, including cells, cell debris, microvesicles, and apoptotic bodies, the collected conditioned media were centrifuged at 1,300 rpm for 3 min followed by filtering with a 0.22 μm vacuum filter/storage bottle system. EVs were isolated using tangential flow filtration (TFF; Repligen, Waltham, MA, USA) with a 500 kDa molecular weight cutoff filter and a diafiltration rate of 7. The isolated EVs were then concentrated for further applications using an Amicon Ultra-15 centrifugal Filter Unit (Merck, Darmstadt, Germany).

Preparation of NAM-Loaded Liposome (LNP). Liposomes were synthesized using the thin film hydration followed by an extrusion method. The lipid components (DOPC: DOTAP: DSPE-mal: NBD-PE: rhodamine-PE = 74:20:4:1:1), containing the fusogenic lipid, were dissolved in chloroform and then dried for 15 min at 60 °C using a rotary evaporator under a constant vacuum. The resulting thin film was resuspended in a PBS solution containing nicotinamide (NAM) until the lipid membrane was fully hydrated. The NAM encapsulated liposome (LNP) was formed by passing the mixture 11 times through a polycarbonate membrane with 100 nm pore sizes with a mini extruder (Avanti Polar Lipids, AL, USA). To remove free drugs, the extruded solution was purified three times by using the Amicon ultra-15 centrifugal filter unit (Merck, Darmstadt, Germany).

Characterization of EVs, LNPs, and Hybrid Nanoparticles. The MONO ZetaView (PMX-120, Particle Metrix, Meerbusch, Germany) was employed by using a 488 nm scatter mode to assess the quantity and size of particles. Samples were diluted in filtered phosphate-buffered saline (PBS) solution (HyClone laboratories, UT, USA) to a concentration of 10^7–10^8 particles/mL. Standardized parameters, including sensitivity (75), shutter (100), minimum trace length (15), and cell temperature (25 °C), were adjusted for the accurate analysis of all samples. The zeta potential of the particles was determined using a Zetasizer Nano ZS (Malvern, Worcestershire, UK). Transmission electron microscopy (TEM; Hitachi, H^{-7600}, 80 kV, Japan) was utilized to visualize particle morphologies. The particle solution was dried on a Formvar/copper grid coated with carbon (150 mesh, FCF150-CU, Electron Microscopy Sciences, PA, USA). EVs were stained with either 7% uranyl acetate or a gadolinium acetate solution and subsequently dried for negative staining on a copper grid. After drying, the Formvar/copper grid was mounted on the grid box for TEM examination.

TUNEL Analysis. The PRCs were seeded in a 24-well culture plate (5×10^4 cells). PRCs were fixed, permeabilized, and detected according to the protocol provided by the manufacturer. PRCs subjected to the TUNEL assay (25879, Cell Signaling Technologies, MA, USA) were imaged using a fluorescence microscope (CKX53, OLYMPUS, Tokyo, Japan).

Western Blot Analysis. In the Western blot analysis, an equal number of EVs or proteins were used to compare protein expression levels in parallel. After separation using 10% SDS-PAGE, the proteins were transferred onto nitrocellulose (NC) membranes. The NC membrane was blocked with a TBST solution diluted with 5% skim milk. The protein-transferred NC membranes were incubated with primary antibodies against the His tag (ABM, Richmond, BC, Canada), CD63 (Abcam, MA, USA), TSG101, Apo-A1 (Santa Cruz Biotechnology, CA, USA), Col2A1 (sc-52658, Santa Cruz Biotechnology, CA, USA), MMP13 (PA5–27242, Thermo Fisher Scientific, OH, USA), and β-actin (sc-47778, Santa Cruz Biotechnology, CA, USA), respectively. These were followed by incubation with HRP-linked secondary antibodies (Cell Signaling Technology, MA, USA). The blot was then treated with enhanced chemiluminescence solution (GE Healthcare, WI, USA) and visualized using the ChemiDoc XRS+ system and ImageLab software (Bio-Rad, CA, USA).

Particle Hybridization & FRET Analysis. To achieve ethanol-mediated hybridization, the same number of EVs and LNPs, quantified using MONO ZetaView, were mixed and incubated for 1 h in 30% ethanol. After a 1 h incubation, a PBS solution was added to stop the ethanol-induced reaction. To remove the ethanol and concentrate the particles, the mixture was processed using the Amicon ultra-15 centrifugal filter unit (Merck, Darmstadt, Germany). To confirm hybridization with FRET-based analysis, two separate fluorophore-labeled lipids, NBD-PE and rhodamine-PE were utilized to form LNPs. The fluorescence profiles were detected with a microplate reader (Molecular Devices, CA, USA) at the three respect wavelengths (excitation at 460 nm, emission at 540 and 590 nm, cutoff at 530 nm). The emission point was determined by measuring the lambda maxima of NBD-PE and Rhodamine-PE. FRET intensity was calculated using the following equation, $(F_{590}/(F_{540} + F_{590})) \times 100$, where F_{540} = emission fluorescence at 540 nm and where F_{590} = emission fluorescence at 590 nm.

Wound Healing Assay in the Primary Rat Chondrocyte (PRC). The primary rat chondrocytes (PRCs) were cultured in 6-well plates at a density of 5×10^5 cells per well until they formed a confluent monolayer. A sterile 1 mL pipet tip was used to scratch the center of the wells. After rinsing with PBS solution, the cells were treated with four different nanoparticles, EVs, LNPs, EVs+LNPs, and N-Hybrid, at a concentration of 1×10^8 particles/mL. Wound healing activity was monitored 24 h later using a microscopy. The percentage of open area was calculated using the wound healing tool plugin in ImageJ (Wayne Rasband, NIH, USA).

Immunocytochemistry (ICC). The PRCs were fixed in 4% paraformaldehyde at room temperature for 20 min. To increase cell permeability, cells were treated with 0.2% Triton-X diluted in a PBS solution for 10 min at the same temperature. Subsequently, the cells were blocked with 1% BSA in PBS solution and incubated overnight at 4 °C with the primary antibody followed by incubating for an additional 1 h with the secondary antibody at room temperature in the dark condition. The antibodies, including NF-κB primary antibody (SC-8008, 2 μg/mL, Santa Cruz Biotechnology, CA, USA) and MMP13 (PA5–27242, Thermo Fisher Scientific, OH, USA), were employed for immunofluorescence labeling. Secondary

https://doi.org/10.1021/acsnano.4c07992
ACS Nano 2024, 18, 33937–33952

antibodies were goat antimouse IgG (H+L) cross-adsorbed secondary antibody, Alexa fluor 555 (A-21422, 200:1, Invitrogen, CA, USA), donkey antirabbit IgG (H+L), and Alexa Fluor 488 (A-21206, 200:1, Invitrogen, CA, USA). Hoechst stain (62249, 1 μg/mL, Thermo Fisher Scientific, OH, USA) was used for nuclear staining. Fluorescence microscopy (CKX53, OLYMPUS, Tokyo, Japan) was employed for image acquisition.

Enzyme-Linked Immunosorbent Assay (ELISA). The presence of TGF-β1 in EVs and N-Hybrid was verified using the human TGF-beta 1 DuoSet ELISA kit (DY240, R&D Systems, MN, USA). Equal numbers of particles (1×10^9 particles) were added to ELISA wells, and the assay was performed following the manufacturer's protocol. Absorbance was detected at 450 nm using a microplate reader (Molecular Devices, CA, USA) with background subtraction measured at wavelengths of 540 and 570 nm.

Antibody Engineering. Generating and purifying $F(ab')_2$ fragments of Col2A1 antibody was carried out using the Pierce $F(ab')_2$ Preparation Kit (44988, Thermo Fisher Scientific, MA, USA). The Col2A1 antibody was processed using immobilized pepsin to separate $F(ab')_2$ fragments and Fc fragments. The resulting $F(ab')_2$ fragments were processed, purified, and separated according to the manufacturer's instructions. Subsequently, dithiothreitol (DTT, 0.5 mM) was applied for 30 min at room temperature to generate sulfhydryl groups on the antibody fragments for conjugation with the maleimide groups on Mal-LNP. Free DTT was completely removed from the reaction buffers using Zeba spin desalting columns (89882, Thermo Fisher Scientific, MA, USA). Finally, the conjugation was conducted with a concentration of 25 μg Col2A1 $F(ab')_2$ per 1 mg LNPs for 2 h at room temperature.[66]

Evaluation of Particle Affinity to Femoral Condyle. The femoral condyle was harvested from Sprague–Dawley (SD) rats, washed with PBS solution, and treated with 0.25% trypsin-EDTA (TE) for 1 h. After incubation with TE, the damaged femoral condyle was rinsed with a PBS solution. To visualize N-Hybrid and Ab-Hybrid, they were incubated with a Vybrant DiD cell-labeling solution (Thermo Fisher Scientific, MA, USA) for 30 min. An *ex vivo* osteoarthritis mimicking model was prepared, and both N-Hybrid and Ab-Hybrid (1×10^{10} particles) were treated to damaged chondrocytes for 1 h to compare their affinity. The affinity of particles to the femoral condyle was evaluated by measuring the DiD intensity using a fluorescence-labeled organism bioimaging instrument (FOBI; Neoscience, Seoul, Korea). The DiD intensity was then normalized based on the area of the femoral condyle for parallel comparisons.

RT-qPCR for Regulation of Osteoarthritis-Related Factors. PRCs were seeded at a density of 5×10^5 cells/well in 6-well plates for the *in vitro* experiment. An equal number of nanoparticles were treated for 24 h after TNF-α (20 ng/mL) pretreatment to induce damages for PRCs. RNA for qPCR (quantitative real-time PCR) was extracted to determine the levels of inflammation and regeneration. Additionally, the knee cartilage isolated from SD rats was frozen using liquid nitrogen and subsequently powdered for *in vivo* test. RNA extraction was then performed using the TRIzol Reagent. The SYBR green PCR reagent mix (Applied Biosystems, CA, USA) was applied to real-time PCR. QuantStudio 3 (Applied Biosystems, CA, USA) was employed to perform reactions with the following primers. MMP13: forward, 5′-ctgcggttcactttgaggac-3′ and reverse, 5′-acagcatc-tactttgtcgcc-3′; Col2: forward, 5′-caccgctaacgtccagatgac-3′ and reverse, 5′-ggaaggcgtgaggtcttctgt-3′; NF-kB: forward, 5′-ccgggatggcttctatgag-3′, and reverse, 5′-ccgtctttctgtcacggtct-3′; IL-6: forward, 5′- cctggagtttgtgaagaacaact-3′ and reverse, 5′-ggaagttgggg-taggaagga-3′; 18 s rRNA: forward, 5′- gtggttttcggaactgaggc-3′ and reverse, 5′-gtcggcatcgtttatggtcg-3′. The data were quantified using $2^{-\Delta\Delta Ct}$ method with 18 s rRNA as a reference.

Animal Test and Histological Analysis. All animal procedures complied with the laboratory animal management and use guidelines of CHA University and were approved by the Institutional Animal Care and Use Committee (IACUC230176). Eight-week-old male Sprague–Dawley (SD) rats (Raon Bio, Yongin, Korea) were used for the study. The SD rats were anesthetized using isoflurane (Terrell Isoflurane, Piramal Critical Care Inc., Bethlehem, PA, USA). The SD rats were subjected to surgery for destabilization of the medial meniscus (DMM) using a previously described protocol.[58] For particle tracking, DiD-labeled N-Hybrid and Ab-Hybrid (1×10^{10} particles) were injected into the joint cavity at SD rat 6 weeks after DMM modeling, and *in vivo* imaging was performed with Davinci-Invivo imaging system (Davinch-k, Seoul, Korea) until 60 days when all particles disappeared in both groups (excitation: 640 nm emission: 680 nm). After the animals were euthanized, tissue samples were embedded in paraffin and sectioned into 10 μm slices, and these sections were stained with hematoxylin and eosin (H&E; Abcam, MA, USA) and Safranin O-fast green (S/O; IHC WORLD, Woodstock, MD, USA) according to the manufacturer's instructions.

Statistical Analysis. Statistical analyses were conducted using GraphPad Prism 7 software (GraphPad Prism 7.00 Software, La Jolla, CA, USA). Differences among groups were evaluated using unpaired *t*-tests or one-way analysis of variance (ANOVA) followed by Tukey's multiple comparison post-test for comparisons involving more than three groups. Statistical significance was defined as p values less than 0.05 (* $p < 0.05$; ** $p < 0.01$; *** $p < 0.001$; **** $p < 0.0001$).

ASSOCIATED CONTENT

Supporting Information

The Supporting Information is available free of charge at https://pubs.acs.org/doi/10.1021/acsnano.4c07992.

Inhibitory effect of nicotinamide (NAM) on inflammation-induced apoptosis (TUNEL assay); HPLC standard curve of nicotinamide (NAM); polydispersity index (PDI) measurement of particles using dynamic light scattering (DLS); comparative analysis of EV markers in TGF-β1 EV, N-Hybrid, and Ab-Hybrid (Western blot); evaluation of particle affinity in N-Hybrid and Ab-Hybrid; image of the joint region with DMM (destabilization of the medial meniscus) modeling; and image of the joint region with DMM (destabilization of the medial meniscus) modeling (PDF)

AUTHOR INFORMATION

Corresponding Author

Dong Keun Han − *Department of Biomedical Science, CHA University, Seongnam-si, Gyeonggi-do 13488, Republic of Korea;* orcid.org/0000-0003-4641-7883; Email: dkhan@cha.ac.kr

Authors

Jun Yong Kim − *Department of Biomedical Science, CHA University, Seongnam-si, Gyeonggi-do 13488, Republic of Korea; Department of Biomedical Engineering and Intelligent Precision of Healthcare Convergence, SKKU Institute for Convergence, Sungkyunkwan University (SKKU), Suwon-si, Gyeonggi-do 16419, Republic of Korea;* orcid.org/0000-0001-8659-6623

Won-Kyu Rhim − *Department of Biomedical Science, CHA University, Seongnam-si, Gyeonggi-do 13488, Republic of Korea; Department of Ophthalmology, CHA Bundang Medical Center, CHA University, Seongnam-si 13496, Republic of Korea*

Seung Yeon Lee − *Department of Biomedical Science, CHA University, Seongnam-si, Gyeonggi-do 13488, Republic of Korea*

Jung Min Park − *Department of Biomedical Science, CHA University, Seongnam-si, Gyeonggi-do 13488, Republic of Korea*

https://doi.org/10.1021/acsnano.4c07992
ACS Nano 2024, 18, 33937−33952

Duck Hyun Song − *Department of Biomedical Science, CHA University, Seongnam-si, Gyeonggi-do 13488, Republic of Korea*
Seung-Gyu Cha − *Department of Biomedical Science, CHA University, Seongnam-si, Gyeonggi-do 13488, Republic of Korea*
Sang-Hyuk Lee − *Department of Biomedical Science, CHA University, Seongnam-si, Gyeonggi-do 13488, Republic of Korea*
Dong-Youn Hwang − *Department of Biomedical Science, CHA University, Seongnam-si, Gyeonggi-do 13488, Republic of Korea*
Byoung Ju Kim − *ATEMs, Seoul-si 05836, Republic of Korea*
Seungsoo Rho − *Department of Ophthalmology, CHA Bundang Medical Center, CHA University, Seongnam-si 13496, Republic of Korea*
Tae-Keun Ahn − *Department of Orthopedic Surgery, CHA Bundang Medical Center CHA University, Seongnam-si 13496, Republic of Korea*
Chun Gwon Park − *Department of Biomedical Engineering and Intelligent Precision of Healthcare Convergence, SKKU Institute for Convergence, Sungkyunkwan University (SKKU), Suwon-si, Gyeonggi-do 16419, Republic of Korea*

Complete contact information is available at: https://pubs.acs.org/10.1021/acsnano.4c07992

Author Contributions

†J.Y.K., W.-K.R., and S.Y.L. contributed equally to this work.

Notes

The authors declare no competing financial interest.

ACKNOWLEDGMENTS

This work was supported by the National Research Foundation of Korea (NRF) grant funded by the Korean Government (MSIT) (no. 2023R1A2C3003807) and the Basic Science Research Program through the National Research Foundation of Korea (NRF) funded by the Ministry of Education (2022R1I1A1A01068486). Also, this research was supported by the Korean Fund for Regenerative Medicine (KFRM) grant funded by the Korean Government (the Ministry of Science and ICT, the Ministry of Health and Welfare (23A0206L1).

REFERENCES

(1) Hunter, D. J.; Bierma-Zeinstra, S. Osteoarthritis. *Lancet* **2019**, *393* (10182), 1745−1759.
(2) Son, Y. O.; Park, S.; Kwak, J. S.; Won, Y.; Choi, W. S.; Rhee, J.; Chun, C. H.; Ryu, J. H.; Kim, D. K.; Choi, H. S.; Chun, J. S. Estrogen-Related Receptor γ Causes Osteoarthritis by Upregulating Extracellular Matrix-Degrading Enzymes. *Nat. Commun.* **2017**, *8* (1), 1−11.
(3) Haviv, Y.; Mazor, S.; Shani, M.; Yanko, R.; Aframian, D. J.; Zadik, Y.; Ben-David, S.; Wilensky, A.; Sharav, Y. The Impact of Expectation for Pain Relief on Orofacial Pain Treatment Outcomes. *Front. Psychiatry* **2021**, *12* (November), 1−6.
(4) Küçükdeveci, A. A. Rehabilitation Interventions in Osteoarthritis. *Best Pract. Res. Clin. Rheumatol.* **2023**, *37* (2), No. 101846.
(5) Guermazi, A.; Neogi, T.; Katz, J. N.; Kwoh, C. K.; Conaghan, P. G.; Felson, D. T.; Roemer, F. W. Intra-Articular Corticosteroid Injections for the Treatment of Hip and Knee Osteoarthritis-Related Pain: Considerations and Controversies with a Focus on Imaging-Radiology Scientific Expert Panel. *Radiology* **2020**, *297* (3), 503−512.
(6) Dou, H.; Wang, S.; Hu, J.; Song, J.; Zhang, C.; Wang, J.; Xiao, L. Osteoarthritis Models: From Animals to Tissue Engineering. *J. Tissue Eng.* **2023**, *14*, 1−23.
(7) McAlindon, T. E.; Bannuru, R. R.; Sullivan, M. C.; Arden, N. K.; Berenbaum, F.; Bierma-Zeinstra, S. M.; Hawker, G. A.; Henrotin, Y.; Hunter, D. J.; Kawaguchi, H.; Kwoh, K.; Lohmander, S.; Rannou, F.; Roos, E. M.; Underwood, M. OARSI Guidelines for the Non-Surgical Management of Knee Osteoarthritis. *Osteoarthr. Cartil.* **2014**, *22* (3), 363−388.
(8) Pelletier, J. P.; Raynauld, J. P.; Abram, F.; Dorais, M.; Paiement, P.; Martel-Pelletier, J. Intra-Articular Corticosteroid Knee Injection Induces a Reduction in Meniscal Thickness with No Treatment Effect on Cartilage Volume: A Case−Control Study. *Sci. Rep.* **2020**, *10* (1), 1−10.
(9) Syed, H. M.; Green, L.; Bianski, B.; Jobe, C. M.; Wongworawat, M. D. Bupivacaine and Triamcinolone May Be Toxic to Human Chondrocytes: A Pilot Study. *Clin. Orthop. Relat. Res.* **2011**, *469* (10), 2941−2947.
(10) Fan, M.; Zhang, J.; Zhou, L.; Chen, Z.; Bao, R.; Zheng, L.; Tong, P.; Ma, Y.; Shan, L. Intra-Articular Injection of Placental Mesenchymal Stromal Cells Ameliorates Pain and Cartilage Anabolism/Catabolism in Knee Osteoarthritis. *Front. Pharmacol.* **2022**, *13*, 1−14.
(11) Epanomeritakis, I. E.; Lee, E.; Lu, V.; Khan, W. The Use of Autologous Chondrocyte and Mesenchymal Stem Cell Implants for the Treatment of Focal Chondral Defects in Human Knee Joints—A Systematic Review and Meta-Analysis. *Int. J. Mol. Sci.* **2022**, *23* (7), 4065.
(12) Kim, J. Y.; Rhim, W. K.; Yoo, Y. I.; Kim, D. S.; Ko, K. W.; Heo, Y.; Park, C. G.; Han, D. K. Defined MSC Exosome with High Yield and Purity to Improve Regenerative Activity. *J. Tissue Eng.* **2021**, *12*, 1−15.
(13) Rhim, W. K.; Woo, J.; Kim, J. Y.; Lee, E. H.; Cha, S. G.; Kim, D. S.; Baek, S. W.; Park, C. G.; Kim, B. S.; Kwon, T. G.; Han, D. K. Multiplexed PLGA Scaffolds with Nitric Oxide-Releasing Zinc Oxide and Melatonin-Modulated Extracellular Vesicles for Severe Chronic Kidney Disease. *J. Adv. Res.* **2024**.
(14) Kim, J. Y.; Rhim, W. K.; Seo, H. J.; Lee, J. Y.; Park, C. G.; Han, D. K. Comparative Analysis of MSC-Derived Exosomes Depending on Cell Culture Media for Regenerative Bioactivity. *Tissue Eng. Regen. Med.* **2021**, *18* (3), 355−367.
(15) Cha, S. G.; Rhim, W. K.; Kim, J. Y.; Lee, E. H.; Lee, S. Y.; Park, J. M.; Lee, J. E.; Yoon, H.; Park, C. G.; Kim, B. S.; Kwon, T. G.; Lee, Y.; Lee, D. R.; Han, D. K. Kidney Tissue Regeneration Using Bioactive Scaffolds Incorporated with Differentiating Extracellular Vesicles and Intermediate Mesoderm Cells. *Biomater. Res.* **2023**, *27* (1), 1−20.
(16) Lee, S. Y.; Park, J. M.; Rhim, W. K.; Lee, E. H.; Lee, S. H.; Kim, J. Y.; Cha, S. G.; Lee, S. H.; Kim, B.; Hwang, D. Y.; Rho, S.; Ahn, T. K.; Kim, B. S.; Han, D. K. Multifunctional Extracellular Vesicles and Edaravone-Loaded Scaffolds for Kidney Tissue Regeneration by Activating GDNF/RET Pathway. *Nano Converg.* **2024**, *11* (1), 43.
(17) Citro, V.; Clerici, M.; Boccaccini, A. R.; Della Porta, G.; Maffulli, N.; Forsyth, N. R. Tendon Tissue Engineering: An Overview of Biologics to Promote Tendon Healing and Repair. *J. Tissue Eng.* **2023**, *14*, 1−24.
(18) Koh, H. B.; Kim, H. J.; Kang, S. W.; Yoo, T. H. Exosome-Based Drug Delivery: Translation from Bench to Clinic. *Pharmaceutics* **2023**, *15* (8), 2042.
(19) Kim, J. Y.; Rhim, W. K.; Cha, S. G.; Woo, J.; Lee, J. Y.; Park, C. G.; Han, D. K. Bolstering the Secretion and Bioactivities of Umbilical Cord MSC-Derived Extracellular Vesicles with 3D Culture and Priming in Chemically Defined Media. *Nano Converg.* **2022**, *9* (1), 1−18.
(20) Kim, J. Y.; Rhim, W. K.; Woo, J.; Cha, S. G.; Park, C. G.; Han, D. K. The Upregulation of Regenerative Activity for Extracellular Vesicles with Melatonin Modulation in Chemically Defined Media. *Int. J. Mol. Sci.* **2022**, *23* (23), 15089.
(21) Kar, R.; Dhar, R.; Mukherjee, S.; Nag, S.; Gorai, S.; Mukerjee, N.; Mukherjee, D.; Vatsa, R.; Chandrakanth Jadhav, M.; Ghosh, A.; Devi, A.; Krishnan, A.; Thorat, N. D. Exosome-Based Smart Drug

Delivery Tool for Cancer Theranostics. *ACS Biomater. Sci. Eng.* **2023**, *9* (2), 577−594.
(22) Ji, K.; Fan, M.; Huang, D.; Sun, L.; Li, B.; Xu, R.; Zhang, J.; Shao, X.; Chen, Y. Clodronate-Nintedanib-Loaded Exosome-Liposome Hybridization Enhances the Liver Fibrosis Therapy by Inhibiting Kupffer Cell Activity. *Biomater. Sci.* **2022**, *10* (3), 702−713.
(23) Hu, Y.; Li, X.; Zhang, Q.; Gu, Z.; Luo, Y.; Guo, J.; Wang, X.; Jing, Y.; Chen, X.; Su, J. Exosome-Guided Bone Targeted Delivery of Antagomir-188 as an Anabolic Therapy for Bone Loss. *Bioact. Mater.* **2021**, *6* (9), 2905−2913.
(24) Liu, A.; Yang, G.; Liu, Y.; Liu, T. Research Progress in Membrane Fusion-Based Hybrid Exosomes for Drug Delivery Systems. *Front. Bioeng. Biotechnol.* **2022**, *10* (August), 1−14.
(25) Gonda, A.; Kabagwira, J.; Senthil, G. N.; Wall, N. R. Internalization of Exosomes through Receptor-Mediated Endocytosis. *Mol. Cancer Res.* **2019**, *17* (2), 337−347.
(26) Chan, M. H.; Chang, Z. X.; Huang, C. Y. F.; Lee, L. J.; Liu, R. S.; Hsiao, M. Integrated Therapy Platform of Exosomal System: Hybrid Inorganic/Organic Nanoparticles with Exosomes for Cancer Treatment. *Nanoscale Horizons* **2022**, *7* (4), 352−367.
(27) Guo, X.; Xi, L.; Yu, M.; Fan, Z.; Wang, W.; Ju, A.; Liang, Z.; Zhou, G.; Ren, W. Regeneration of Articular Cartilage Defects: Therapeutic Strategies and Perspectives. *J. Tissue Eng.* **2023**, *14*, 1−27.
(28) Hou, X.; Zaks, T.; Langer, R.; Dong, Y. Lipid Nanoparticles for MRNA Delivery. *Nat. Rev. Mater.* **2021**, *6* (12), 1078−1094.
(29) Nguyen, J.; Fuhrmann, G. Extracellular Vesicles — A Versatile Biomaterial. *Adv. Healthc. Mater.* **2022**, *11* (5), 1−3.
(30) Shao, Z.; Xu, J.; Xu, X.; Wang, X.; Zhou, Y.; Li, Y.; Li, K. Exosomes Derived from Human Adipose Mesenchymal Stem Cells Inhibits Fibrosis and Treats Oral Submucous Fibrosis via the MiR-181a-5p/Smad2 Axis. *Tissue Eng. Regen. Med.* **2024**, *21* (1), 123−135.
(31) Kim, H. J.; Kim, G.; Lee, J.; Lee, Y.; Kim, J. H. Secretome of Stem Cells: Roles of Extracellular Vesicles in Diseases, Stemness, Differentiation, and Reprogramming. *Tissue Eng. Regen. Med.* **2022**, *19* (1), 19−33.
(32) Mengstie, M. A.; Wondimu, B. Z. Mechanism and Applications of Crispr/ Cas-9-Mediated Genome Editing. *Biol. Targets Ther.* **2021**, *15*, 353−361.
(33) Malekian, F.; Shamsian, A.; Kodam, S. P.; Ullah, M. Exosome Engineering for Efficient and Targeted Drug Delivery: Current Status and Future Perspective. *J. Physiol.* **2023**, *601* (22), 4853−4872.
(34) Sahin, K.; Kucuk, O.; Orhan, C.; Tuzcu, M.; Durmus, A. S.; Ozercan, I. H.; Sahin, N.; Juturu, V. Niacinamide and Undenatured Type II Collagen Modulates the Inflammatory Response in Rats with Monoiodoacetate-Induced Osteoarthritis. *Sci. Rep.* **2021**, *11* (1), 1−15.
(35) Kim, M.; Kim, J. Y.; Rhim, W. K.; Cimaglia, G.; Want, A.; Morgan, J. E.; Williams, P. A.; Park, C. G.; Han, D. K.; Rho, S. Extracellular Vesicle Encapsulated Nicotinamide Delivered via A Trans-Scleral Route Provides Retinal Ganglion Cell Neuroprotection. *Acta Neuropathol. Commun.* **2024**, *12* (1), 1−16.
(36) Cao, C.; Shi, Y.; Zhang, X.; Li, Q.; Zhang, J.; Zhao, F.; Meng, Q.; Dai, W.; Liu, Z.; Yan, W.; Duan, X.; Zhang, J.; Fu, X.; Cheng, J.; Hu, X.; Ao, Y. Cholesterol-Induced LRP3 Downregulation Promotes Cartilage Degeneration in Osteoarthritis by Targeting Syndecan-4. *Nat. Commun.* **2022**, *13* (1), 1−16.
(37) Bedingfield, S. K.; Colazo, J. M.; Yu, F.; Liu, D. D.; Jackson, M. A.; Himmel, L. E.; Cho, H.; Crofford, L. J.; Hasty, K. A.; Duvall, C. L. Amelioration of Post-Traumatic Osteoarthritis via Nanoparticle Depots Delivering Small Interfering RNA to Damaged Cartilage. *Nat. Biomed. Eng.* **2021**, *5* (9), 1069−1083.
(38) Lee, H. I.; Rhim, W. K.; Kang, E. Y.; Choi, B.; Kim, J. H.; Han, D. K. A Multilayer Functionalized Drug-Eluting Balloon for Treatment of Coronary Artery Disease. *Pharmaceutics* **2021**, *13* (5), 614−16.
(39) Seo, H. J.; Rhim, W. K.; Baek, S. W.; Kim, J. Y.; Kim, D. S.; Han, D. K. Endogenous Stimulus-Responsive Nitric Oxide Releasing Bioactive Liposome for a Multilayered Drug-Eluting Balloon. *Biomater. Sci.* **2023**, *11* (3), 916−930.
(40) Cavalcanti, R. R. M.; Lira, R. B.; Riske, K. A. Membrane Fusion Biophysical Analysis of Fusogenic Liposomes. *Langmuir* **2022**, *38* (34), 10430.
(41) Rhim, W. K.; Kim, J. Y.; Lee, S. Y.; Cha, S. G.; Park, J. M.; Park, H. J.; Park, C. G.; Han, D. K. Recent Advances in Extracellular Vesicle Engineering and Its Applications to Regenerative Medicine. *Biomater. Res.* **2023**, *27* (1), 1−31.
(42) Piffoux, M.; Silva, A. K. A.; Wilhelm, C.; Gazeau, F.; Tareste, D. Modification of Extracellular Vesicles by Fusion with Liposomes for the Design of Personalized Biogenic Drug Delivery Systems. *ACS Nano* **2018**, *12* (7), 6830−6842.
(43) Cabanillas, B.; Novak, N.; Akdis, C. A. The Form of PEG Matters: PEG Conjugated with Lipids and Not PEG Alone Could Be the Specific Form Involved in Allergic Reactions to COVID-19 Vaccines. *Allergy Eur. J. Allergy Clin. Immunol.* **2022**, *77* (6), 1658−1660.
(44) Eun Shin, H.; Wook Oh, S.; Park, W. Hybrid Nanovesicle of Chimeric Antigen Receptor (CAR)-Engineered Cell-Derived Vesicle and Drug-Encapsulated Liposome for Effective Cancer Treatment. *J. Ind. Eng. Chem.* **2023**, *122*, 127−137.
(45) Bompard, J.; Rosso, A.; Brizuela, L.; Mebarek, S.; Blum, L. J.; Trunfio-Sfarghiu, A. M.; Lollo, G.; Granjon, T.; Girard-Egrot, A.; Maniti, O. Membrane Fluidity as a New Means to Selectively Target Cancer Cells with Fusogenic Lipid Carriers. *Langmuir* **2020**, *36* (19), 5134−5144.
(46) Zhang, L.; Gao, J.; Qi, A.; Gao, Y. A Novel DRET and FRET Combined Fluorescent Molecule and Its Applications in Sensing and Bioimaging. *Sens.Actuators, B Chem.* **2020**, *320*, No. 128457.
(47) Lin, Y.; Wu, J.; Gu, W.; Huang, Y.; Tong, Z.; Huang, L.; Tan, J. Exosome−Liposome Hybrid Nanoparticles Deliver CRISPR/Cas9 System in MSCs. *Adv. Sci.* **2018**, *5* (4), 1−9.
(48) Rayamajhi, S.; Nguyen, T. D. T.; Marasini, R.; Aryal, S. Macrophage-Derived Exosome-Mimetic Hybrid Vesicles for Tumor Targeted Drug Delivery. *Acta Biomater.* **2019**, *94*, 482−494.
(49) Mukherjee, D.; Paul, D.; Sarker, S.; Hasan, M. N.; Ghosh, R.; Prasad, S. E.; Vemula, P. K.; Das, R.; Adhikary, A.; Pal, S. K.; Rakshit, T. Polyethylene Glycol-Mediated Fusion of Extracellular Vesicles with Cationic Liposomes for the Design of Hybrid Delivery Systems. *ACS Appl. Bio Mater.* **2021**, *4* (12), 8259−8266.
(50) Cheng, L.; Zhang, X.; Tang, J.; Lv, Q.; Liu, J. Gene-Engineered Exosomes-Thermosensitive Liposomes Hybrid Nanovesicles by the Blockade of CD47 Signal for Combined Photothermal Therapy and Cancer Immunotherapy. *Biomaterials* **2021**, *275* (February), No. 120964.
(51) Kim, J. Y.; Lee, S. Y.; Cha, S.; Park, J. M.; Song, D. H.; Lee, S.; Hwang, D.; Kim, B. J.; Rho, S.; Park, C. G.; Rhim, W.; Han, D. K. Combinatory Nanovesicle with SiRNA-Loaded Extracellular Vesicle and IGF-1 for Osteoarthritis Treatments. *Int. J. Mol. Sci.* **2024**, *1−18*, 5242.
(52) Di Francesco, M.; Bedingfield, S. K.; Di Francesco, V.; Colazo, J. M.; Yu, F.; Ceseracciu, L.; Bellotti, E.; Di Mascolo, D.; Ferreira, M.; Himmel, L. E.; Duvall, C.; Decuzzi, P. Shape-Defined MicroPlates for the Sustained Intra-Articular Release of Dexamethasone in the Management of Overload-Induced Osteoarthritis. *ACS Appl. Mater. Interfaces* **2021**, *13* (27), 31379−31392.
(53) Glorieux, F. H.*Pediatric Bone: Biology & Diseases.*; Elsevier, 2003.
(54) Sandberg, M. M.; Hirvonen, H. E.; Elima, K. J. M.; Vuorio, E. I. Co-Expression of Collagens II and XI and Alternative Splicing of Exon 2 of Collagen II in Several Developing Human Tissues. *Biochem. J.* **1993**, *294* (2), 595−602.
(55) Bedingfield, S. K.; Colazo, J. M.; Di Francesco, M.; Yu, F.; Liu, D. D.; Di Francesco, V.; Himmel, L. E.; Gupta, M. K.; Cho, H.; Hasty, K. A.; Decuzzi, P.; Duvall, C. L. Top-Down Fabricated MicroPlates for Prolonged, Intra-Articular Matrix Metalloproteinase 13 SiRNA Nanocarrier Delivery to Reduce Post-Traumatic Osteoarthritis. *ACS Nano* **2021**, 14475.
(56) Lee, N. K.; Wang, C. P. J.; Lim, J.; Park, W.; Kwon, H. K.; Kim, S. N.; Kim, T. H.; Park, C. G. Impact of the Conjugation of

https://doi.org/10.1021/acsnano.4c07992
ACS Nano 2024, 18, 33937−33952

Antibodies to the Surfaces of Polymer Nanoparticles on the Immune Cell Targeting Abilities. *Nano Converg.* **2021**, *8* (1), 24.
(57) Lagarto, J. L.; Nickdel, M. B.; Kelly, D. J.; Price, A.; Nanchahal, J.; Dunsby, C.; French, P.; Itoh, Y. Autofluorescence Lifetime Reports Cartilage Damage in Osteoarthritis. *Sci. Rep.* **2020**, *10* (1), 1−9.
(58) Glasson, S. S.; Blanchet, T. J.; Morris, E. A. The Surgical Destabilization of the Medial Meniscus (DMM) Model of Osteoarthritis in the 129/SvEv Mouse. *Osteoarthr. Cartil.* **2007**, *15* (9), 1061−1069.
(59) Li, G.; Liu, S.; Chen, Y.; Xu, H.; Qi, T.; Xiong, A.; Wang, D.; Yu, F.; Weng, J.; Zeng, H. Teriparatide Ameliorates Articular Cartilage Degradation and Aberrant Subchondral Bone Remodeling in DMM Mice. *J. Orthop. Transl.* **2023**, *38* (July 2022), 241−255.
(60) Qi, F.; Cui, S. L.; Zhang, B.; Li, H. N.; Yu, J. T-2 Toxin-Induced Damage to Articular Cartilage in Rats Coincided with Impaired Autophagy Linked to the HIF-1α/AMPK Signaling Axis. *Toxicon* **2024**, *243* (March), No. 107735.
(61) Wang, P.; Xiong, X.; Zhang, J.; Qin, S.; Wang, W.; Liu, Z. Icariin Increases Chondrocyte Vitality by Promoting Hypoxia-Inducible Factor-1α Expression and Anaerobic Glycolysis. *Knee* **2020**, *27* (1), 18−25.
(62) Shen, K.; Liu, X.; Qin, H.; Chai, Y.; Wang, L.; Yu, B. Ha-g-Cs Implant and Moderate-Intensity Exercise Stimulate Subchondral Bone Remodeling and Promote Repair of Osteochondral Defects in Mice. *Int. J. Med. Sci.* **2021**, *18* (16), 3808−3820.
(63) Pritzker, K. P. H.; Gay, S.; Jimenez, S. A.; Ostergaard, K.; Pelletier, J. P.; Revell, K.; Salter, D.; van den Berg, W. B. Osteoarthritis Cartilage Histopathology: Grading and Staging. *Osteoarthr. Cartil.* **2006**, *14* (1), 13−29.
(64) Zhang, B.; Zhang, Y.; Wu, N.; Li, J.; Liu, H.; Wang, J. Integrated Analysis of COL2A1 Variant Data and Classification of Type II Collagenopathies. *Clin. Genet.* **2020**, *97* (3), 383−395.
(65) Oladazimi, S.; farzanegi, p.; Azarbayejani, M. A. Evaluation of ALK5 and MMP13 Expression in the Cartilage Tissue of Rats with Osteoarthritis Rats and Effects of Exercise Training, Ozone and Mesenchymal Stem Cell Therapies on Expression of These Genes. *Med. Lab. J.* **2020**, *14* (1), 50−56.
(66) Dai, Y.; Song, Y.; Xie, J.; Xiao, G.; Li, X.; Li, Z.; Gao, F.; Zhang, Y.; He, E.; Xu, S.; Wang, Y.; Zheng, W.; Jiang, X.; Qi, Z.; Meng, D.; Fan, Z.; Cai, X. CB1-Antibody Modified Liposomes for Targeted Modulation of Epileptiform Activities Synchronously Detected by Microelectrode Arrays. *ACS Appl. Mater. Interfaces* **2020**, *12* (37), 41148−41156.

https://doi.org/10.1021/acsnano.4c07992
ACS Nano 2024, 18, 33937−33952